



This is the peer reviewed version of the following article:

Balos, V., Marekha, B. A., Malm, C., Wagner, M., Nagata, Y., Bonn, M., et al. (2019). Specific Ion Effects on an Oligopeptide: Bidentate binding matters for the Guanidinium Cation. *Angewandte Chemie International Edition in English*, 58(1), 332-337. doi:10.1002/anie.201811029.

, which has been published in final form at: [10.1002/anie.201811029](https://doi.org/10.1002/anie.201811029)

Specific Ion Effects on an Oligopeptide: Bidentate binding matters for the Guanidinium Cation

Vasileios Balos, Bogdan Marekha, Christian Malm, Manfred Wagner, Yuki Nagata, Mischa Bonn and Johannes Hunger*

Specific Ion Effects on an Oligopeptide: Bidentate binding matters for the Guanidinium Cation

Vasileios Balos,^[a,b] Bogdan Marekha,^[a] Christian Malm,^[a] Manfred Wagner,^[a] Yuki Nagata,^[a] Mischa Bonn^[a] and Johannes Hunger^{[a]*}

^[a] *Max Planck Institute for Polymer Research, Ackermannweg 10, 55128 Mainz, Germany*

^[b] *Present address: Fritz Haber Institute of the Max Planck Society, Faradayweg 4, 14195 Berlin, Germany*

** Email: hunger@mpip-mainz.mpg.de*

Supporting Information

Materials

Triglycine (BioUltra \geq 99% Sigma Aldrich) and the salts KCl (Sigma Aldrich), KI (Sigma Aldrich), KSCN (Sigma Aldrich), LiCl (Sigma Aldrich) and GdmCl (Sigma Aldrich), were used as received. Three different series of solutions were prepared volumetrically: (a) series of aqueous triglycine solutions, which were prepared at concentrations, c_{GGG} , between 0.05 to 0.3 mol·L⁻¹ at increments of 0.05 mol·L⁻¹, (b) ternary solutions of triglycine (0.247 mol·L⁻¹) + water + salt with increasing concentrations of salt, c_{salt} , at 0.05, 0.1, 0.2, 0.3, 0.4, 0.5, 0.6 and 0.75 mol·L⁻¹. These samples were prepared by diluting an aqueous stock solution with a given mass fraction of triglycine with concentrated aqueous salt stock solutions and water. (c) for NMR experiments ternary solutions of triglycine (0.5 mg·mL⁻¹) + D₂O + salt, with the salt concentrations scaling at molar ratios (of triglycine:salt) of 1:0, 1:1, 1:5, 1:10, 1:50, 1:100, 1:500 and 1:1000 were prepared by mixing solutions of salt in D₂O and triglycine in D₂O.

To avoid uptake of moisture, all salt stock solutions of series (b) and (c) were prepared by weighing the appropriate amount of salt in a glove box and subsequently adding Milli-Q water or D₂O (Eurisotope 99.90 % D).

Experimental Methods

Complex permittivity spectra were measured using a combination of two different experiments: We cover frequencies at $0.2 \leq \nu/\text{GHz} \leq 36$ by using a frequency domain reflectometer based on Anritsu Vector Star MS4647A, vector network analyser with an open ended coaxial probe, based on 1.85 mm coaxial connectors.^[1] Frequencies at $56 \leq \nu/\text{GHz} \leq 125$ were covered analogously using an open ended coaxial probe, based on 1 mm coaxial connectors together with an external frequency converter module (Anritsu 3744A mmW module).

To obtain the molar concentration of triglycine in the stock solution we measured its density using a DM45 DeltaRange density meter apparatus from Mettler Toledo.

Dynamic viscosity, η , of the samples of series (a) were determined using a capillary Ubbelohde viscometer (ViskoSystem AVS 370, Schott Instruments, Germany).

¹H-NMR experiments were performed on a 850 MHz Bruker AVANCE III system equipped with a 5 mm triple resonance TXI ¹H/¹³C/¹⁵N probe with a z-gradient. For proton NMR 512 transients using a 9 μ s long 90° pulse and a 17000 Hz spectral width together with a recycling delay of 5 s. For referencing a sealed capillary with DMSO-d₆ was placed inside the 5 mm tube with a small fraction of DMSO-d₅H. The temperature was controlled to 298.3 K with a VTU (variable temperature unit) and an accuracy of +/- 0.1 K and calibrated with a standard ¹H methanol NMR sample using the Topspin 3.1 software (Bruker).

Dielectric relaxation of aqueous Triglycine solutions

We fit the relaxation model described in the main manuscript (eq. 1) to the spectra of all binary samples. The thus extracted parameters for different concentrations of GGG are summarized in Figs. S1 and S2. The relaxation strength of the water relaxation decreases with increasing c_{GGG} (Fig. S1b), which can be fully explained by a reduction of the molar concentration of water, c_{H_2O} : Assuming the effective dipole moment (dipole moment in solution including dipolar correlations) of water, μ_{eff,H_2O} , to be the same as in neat water^[2], we use the Cavell relation^[3] with $j=H_2O$ to calculate the relaxation strength of water, which is expected based on the molar concentration of water, $S_{H_2O}^{\text{Cav}}$:

$$S_j^{\text{Cav}} = \frac{\varepsilon_{s,j}}{\varepsilon_{s,j} + (1 - \varepsilon_{s,j})/3} \cdot \frac{N_A c_j}{3 k_B T \varepsilon_0} \cdot \mu_{\text{eff},j}^2 \quad (\text{S1})$$

, where N_A is the Avogadro's number, k_B the Boltzmann's constant, ε_0 the permittivity of free space, and T the thermodynamic temperature. ε_{s,H_2O} is the static dielectric permittivity relevant to water (see also eq. 1; $\varepsilon_{s,H_2O} = S_{\text{water}} + \varepsilon_\infty$). As can be seen in Fig. S1b, the relaxation strength based on c_{H_2O} (solid red line in Fig. S1b) excellently agrees with the experimental values of S_{water} . The agreement provides evidence for the relaxation of water being rather insensitive to the presence of GGG: Our results suggest that dipolar correlations and water's dipole moment in solutions of GGG and in neat water is essentially the same.

From the extracted amplitudes of the dielectric relaxation of triglycine, S_{GGG} , we obtain the effective dipole moment of GGG, $\mu_{\text{eff},GGG}$, using eq S1 with $j=GGG$ and $\varepsilon_{s,GGG} = S_{GGG} + S_{\text{water}} + \varepsilon_\infty$.

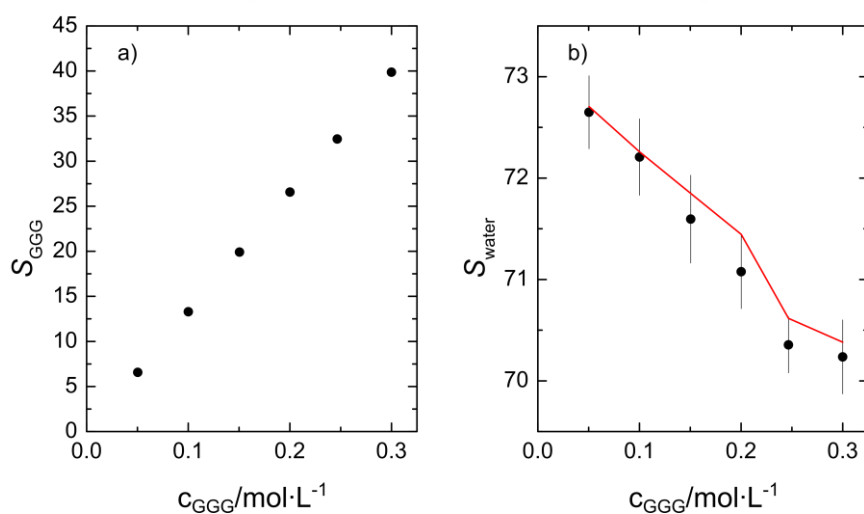


Figure S1. Relaxation amplitudes of a) triglycine (S_{GGG}) and b) water (S_{water}), as obtained by fitting eq.1 to the dielectric spectra of aqueous solutions of GGG. The error bars correspond to the standard deviation within six independent measurements. The solid red line in panel b) shows the relaxation strength $S_{H_2O}^{\text{Cav}}$, which would be expected based on the volume concentration of water (see eq S1).

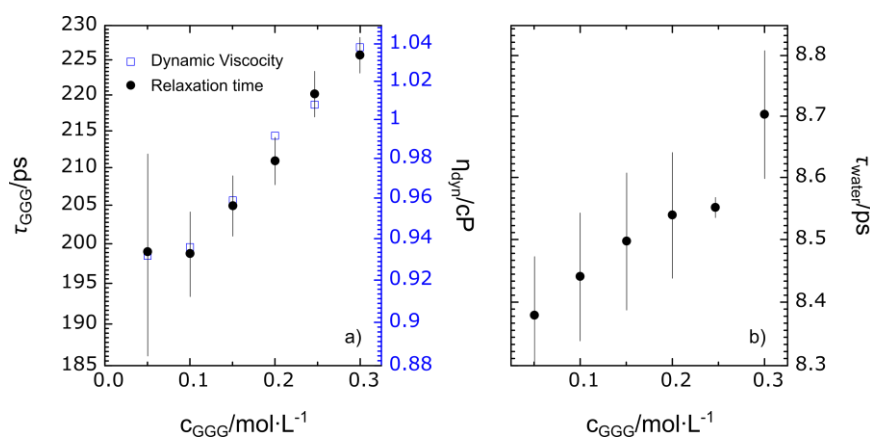


Figure S2. a) Relaxation times of triglycine, τ_{GGG} , (black solid squares) together with the dynamic viscosity, η_{dyn} , of the samples (blue open squares) and b) relaxation time of water (τ_{water}) as a function of triglycine concentration as obtained from fitting eq.1 to the experimental data. The error bars correspond to the standard deviation within six independent measurements.

Molecular dynamics simulation details

All-atom simulations were performed with NAMD 2.12^[4] code using the latest release of the CHARMM C36m additive force-field for GGG and ions in combination with CHARMM modified TIP3P water model.^[5,6] We selected the classical CHARMM force-field due to its well-known transferability^[5] and also because GGG was among the benchmark peptide set used to adjust the backbone dihedral energy terms against experimental J -coupling values.^[6]

Initial structures were prepared with the Molefactory plugin of the VMD 1.9.3 software.^[7] An uncapped GGG zwitterion in a fully stretched conformation (often referred to as β -sheet like or polyglycine^[8]) was placed in the center of a cubic simulation box with 5 nm side length and solvated with either neat TIP3P water or 1 $\text{mol}\cdot\text{L}^{-1}$ LiCl, KCl or GdmCl (75 ion pairs).

Standard three-dimensional periodic boundary conditions were employed. Non-bonded Lennard-Jones and electrostatic interactions were explicitly calculated at each time step between atoms within $r_{\text{cut-off}} = 1.2$ nm distance. The former were smoothly brought to zero at $r_{\text{cut-off}}$ together with the corresponding forces using a switching function at separation distances between 1.0 and 1.2 nm. The neglected long-range contribution to the Lennard-Jones energy term and virial has been accounted for via the corresponding correction.^[9] Long-range (reciprocal) part of the electrostatic interactions was computed using the particle mesh Ewald (PME)^[10] scheme with charges interpolated on a grid with a spacing of approximately 0.1 nm using fifth order B-splines. Neighbour lists for the non-bonded interaction calculation were updated every 20 simulation steps to include atoms within 1.4 nm distance, while the interactions between atoms separated by one or two bonds were excluded and Lennard-Jones interactions between atoms separated by three bonds were scaled according to the CHARMM scheme.^[6] All bond lengths involving hydrogen atoms were kept fixed by means of the SHAKE algorithm^[11] whereas water molecules were maintained rigid using the SETTLE method^[12], which allowed for the use of 2 fs time step with the velocity Verlet integrator.^[13]

The systems were first energy minimized using conjugate gradients method for 5000 steps. They were then subject to 110 ns long constant temperature (300 K) and pressure (1 atm) simulations. The temperature was maintained using Langevin thermostat with the damping coefficient of 5 ps^{-1} while the pressure was controlled via the Langevin piston Nosé-Hoover method^[14,15] as implemented in NAMD with the Langevin piston period of 100 fs and 50 fs decay time. The first 10 ns of the trajectories were discarded as equilibration period and 25000 equally time spaced frames were taken for analysis from the last 100 ns.

In order to confirm that the simulation length employed in the present study is sufficient to sample the relevant conformational states of GGG we calculated the relative Gibbs free energy maps of the two-dimensional probability distribution of the Ramachandran (ϕ , ψ) backbone dihedral angles of the central Gly residue (Fig. S3). Similar distributions were already reported by Best et al.^[6] for C-term protonated GGG from a 400 ns long equilibrium run and by Drake and Montgomery Pettitt^[16] for C- and N-term capped GGG from a 300 ns long trajectory both using C36m force-field and similar simulation set up.

Despite the differences in the termini (fully charged in the present work, partially charged,^[6] or capped^[16]), our results are in excellent agreement with literature reports,^[6,16] since differences in terminal capping and C-term protonation are not expected to have an impact on the Ramachandran distributions of the central residue as long as N-term is not deprotonated.^[17] In particular, we observe essentially equal populations of the right- and left-handed α -helical regions at ($-/+ 75^\circ$; $-/+ 30^\circ$) which are about $1.5 \text{ kcal mol}^{-1}$ less stable than a partially extended polyglycine II (PG II) conformation observed around ($\pm 70^\circ$; $\pm 150^\circ$) while the fully extended polyglycine I conformation (PG I or β) at ($\pm 150^\circ$; $\pm 150^\circ$) is scarcely populated.

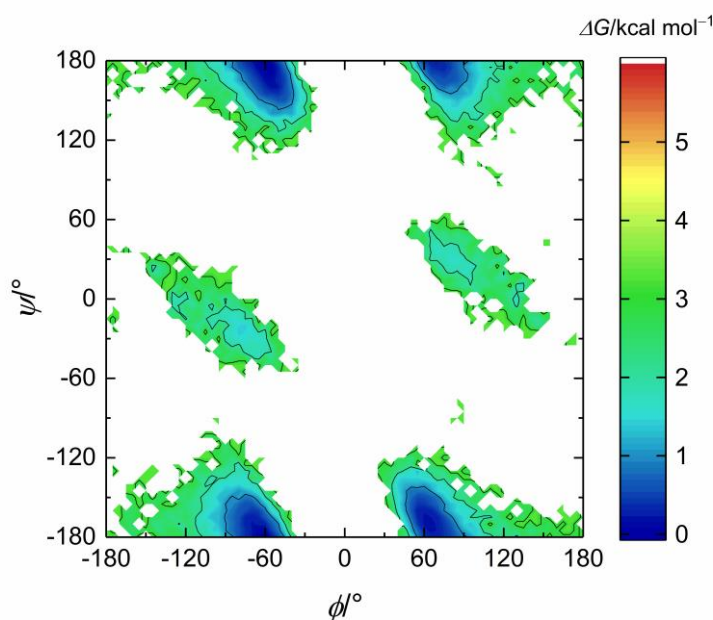


Figure S3. Relative Gibbs free energy contour map of the probability distribution of the Ramachandran (ϕ , ψ) angles of the central Gly residue of GGG zwitter-ion sampled during the last 100 ns of simulation in neat H_2O .

Dielectric relaxation of ternary solutions of triglycine ($0.247 \text{ mol}\cdot\text{L}^{-1}$) + water + salt

We fit the relaxation model described in eq. 1 of the main manuscript to all the experimental data for all salts used and all concentrations. The raw data with the corresponding fits are presented in Fig. S4 (and Fig. 2a of the main manuscript). From such fits we obtain the amplitudes and relaxation times of the triglycine and water relaxations, as well as the conductivity of each sample and the Cole-Cole parameter (α_{CC}) that describes the symmetric broadening of the loss peak of water. All the parameters are presented in the following figures (Figs. S5, S6 and S7).

Similar to our results described above, we estimate the relaxation strength of water. In addition to the reduction of the volume concentration of water (see eq S1), kinetic depolarization reduces water's relaxation strength upon addition of salts. For solutions containing LiCl, strong hydration of LiCl has been reported to further reduce the relaxation strength due to strong hydration of Li^+ .^[18] Thus, if salt

hydration and water dynamics are additive (insensitive to the presence of GGG) the relaxation strength of water can be estimated to:^[19]

$$S_{\text{H}_2\text{O}}^{\text{id}} = S_{\text{H}_2\text{O}}^{\text{Cav}} - \frac{2}{3} \frac{S_{\text{H}_2\text{O}}^{\text{Cav}}}{\epsilon_{\text{s,H}_2\text{O}}} \frac{\tau_{\text{water}}}{\epsilon_0} \kappa - S_{\text{hyd}} \quad (\text{S2})$$

, with the reduction due to hydration, $S_{\text{hyd}} = 0$ for all salts, except for LiCl where we used the values of S_{hyd} determined in Ref. ^[19]. As shown in Fig. S5, the thus determined variation of the relaxation strength agrees well with the experimental values. The minor offset between the two curves, stems from the ambiguity of ϵ_{∞} , which is sensitive to the experimental coverage at high frequencies. This agreement suggests that GGG does not affect the relaxation of water in the electrolyte solutions significantly.

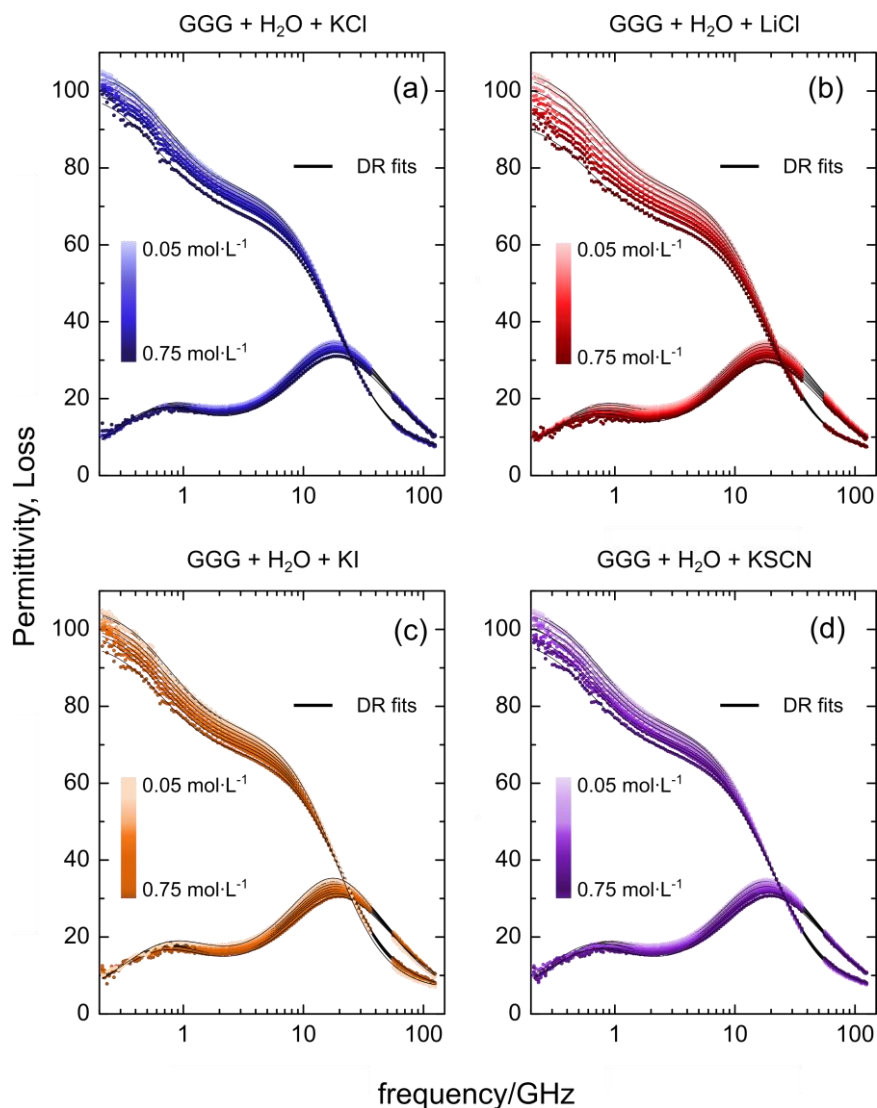


Figure S4. Complex permittivity spectra of mixtures of triglycine and water with increasing concentration (0.05, 0.10, 0.20, 0.30, 0.40, 0.50, 0.60, 0.75 mol·L⁻¹) of (a) KCl, (b) LiCl, (c) KI and (d) KSCN. The symbols correspond to experimental data and the solid lines show fits with the relaxation model described in eq. 1 (main manuscript). The Ohmic loss contribution (last term in eq. 1 has been subtracted for visual clarity).

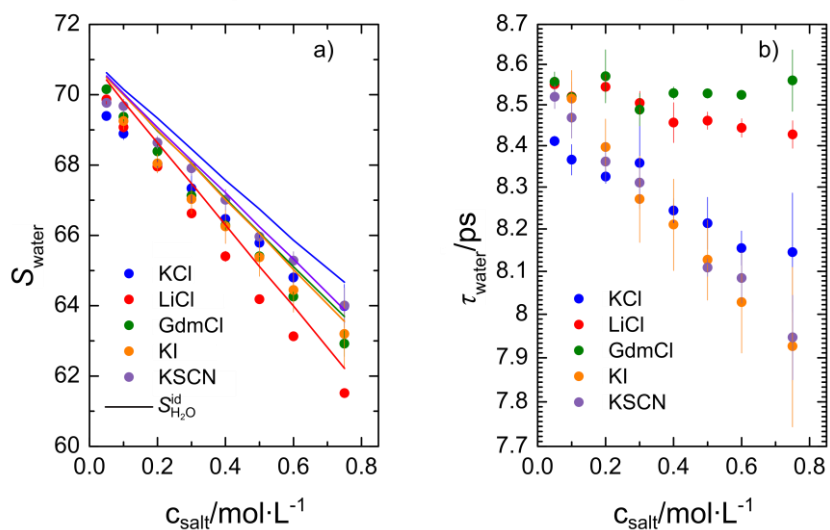


Figure S5. a) Amplitude (S_{water}) and b) relaxation time (τ_{water}) of the water relaxation versus salt concentration, as obtained from fitting eq.1 to the experimental data. The error bars correspond to the standard deviation of six independent measurements. The solid lines in panel a) show the relaxation strength of water that would be expected based on eq S2.

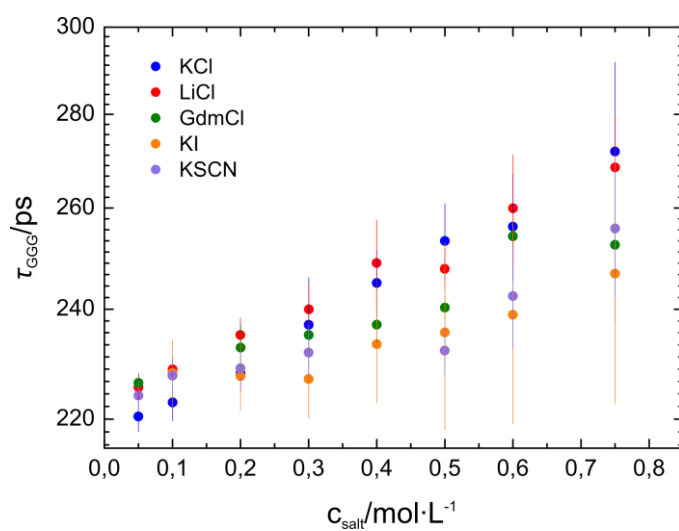


Figure S6. Relaxation time (τ_{GGG}) of the triglycine relaxation versus salt concentration, as obtained from fitting eq.1 to the experimental data. The error bars correspond to the standard deviation of six independent measurements.

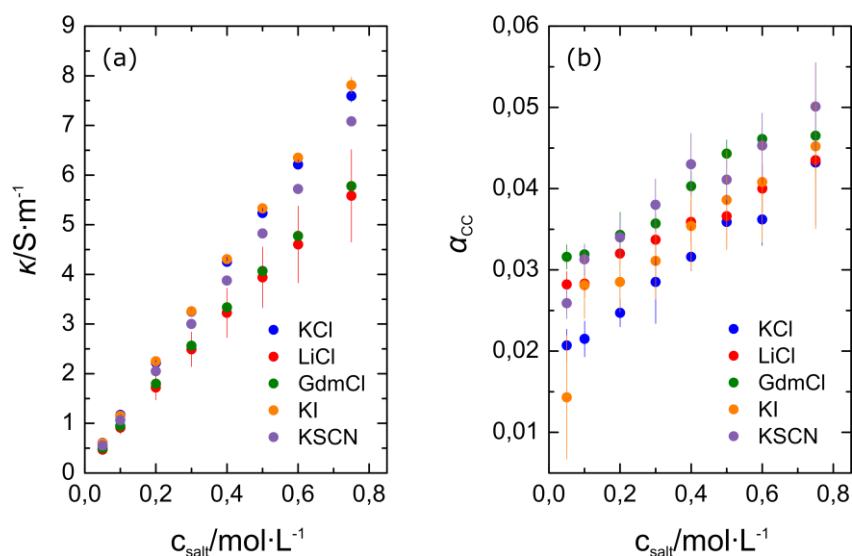


Figure S7. a) Conductivity (κ) and (b) Cole-Cole parameter (α_{CC}) versus salt concentration as obtained from fitting eq. 1 to the experimental data. The error bars correspond to the standard deviation of six independent measurements.

H-NMR measurements of triglycine (0.5 mg/mL) + D₂O + salt

To explore any contribution of specific association of ions to the charged termini of GGG, we performed NMR experiments on GGG in the presence of salts. As has been shown by others,^[20] the variation of the chemical shift, δ , of GGG's CH₂ groups is very sensitive to the immediate environment of the CH₂ protons. For strong association of ions with GGG, the variation of the chemical shift with salt concentration, $\Delta\delta$:

$$\Delta\delta = \delta(c_{\text{salt}} = 0) - \delta(c_{\text{salt}}) \quad (\text{S3})$$

deviates from linearity. A linear variation of the chemical shift can be attributed to a continuous variation of the chemical environment (e.g. linear variation of the volume density of the molecules).^[20] Also weak association equilibria lead to a rather linear variation of the chemical shift.^[21] For strong binding (high corresponding association constants) NMR chemical shifts exhibit marked a non-linear variation with concentration.^[20,21]

The determined values of $\Delta\delta$ of GGG protons for different salts are displayed in Fig. S7. As can be seen from this plot, the chemical shift of the CH₂ groups in the centre of the GGG molecule (position 2) and next to the carboxylate group (position 3) vary linearly with concentration. Hence, we find no evidence for long-lived contacts (strong association) between the studied salts and the amide groups and the carboxylate terminus, respectively. Only for the CH₂ group next to the N-terminus (position 1) $\Delta\delta(c_{\text{salt}})$ somewhat deviated from linearity. However, these deviations neither correlate with the charge of the ions (cation or anion) nor with the nature of the ion. Hence, also from the CH₂ group near the NH₃⁺ group we do not find evidence for significant association of ions to GGG. As such formation of long-lived "ion-pairs" are rendered unlikely based on the NMR chemical shift experiments.

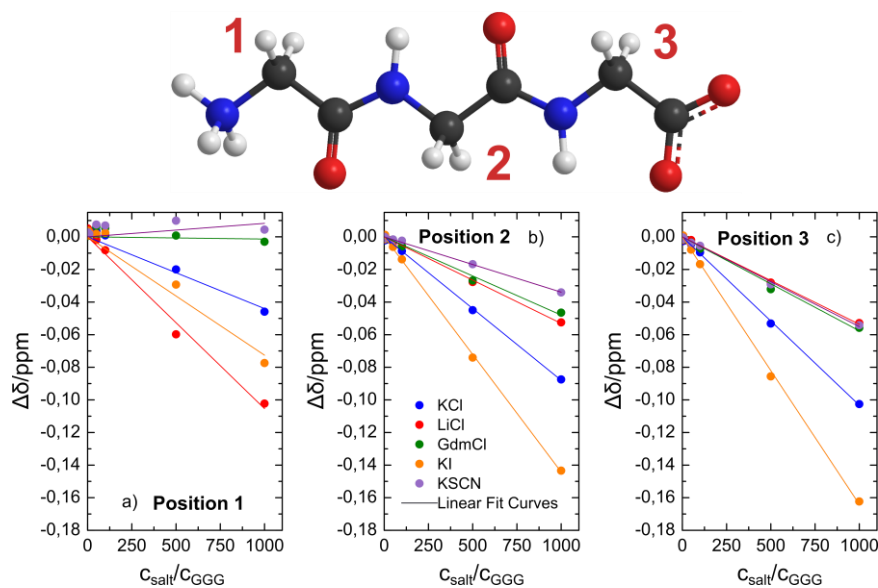


Figure S8. Top: Graphical representation of the GGG zwitterion marked with the positions of the CH₂ groups measured in the NMR. Bottom: Chemical shifts for the three CH₂ positions of GGG versus increasing molar ratios of GGG:salt. The solid lines correspond to best linear fit curves.

CTER^{GGG}-Gdm⁺ vs. Arg/Lys – Asp/Glu

In order to assess the contribution of Gdm⁺-carboxylate interactions to the denaturing ability of Gdm⁺ salts via disruption of Arg/Lys-carboxylate salt bridges and, in a broader sense, ionic interactions in proteins, we compare typical geometries encountered in our MD simulations to the geometries of ionic interactions in folded proteins in the solid state (X-ray structures, Arad et al.^[22] and Donald et al.^[23]) and in solution (NMR resolved structures, Kumar and Nussinov^[24]).

Typical geometrical criteria for a salt bridge are N-O distances shorter than 4.0 Å.^[22–24] This definition covers both strongly interacting multidentate salt bridge motifs (see Figure S9 for examples) as well as weak ionic interactions.

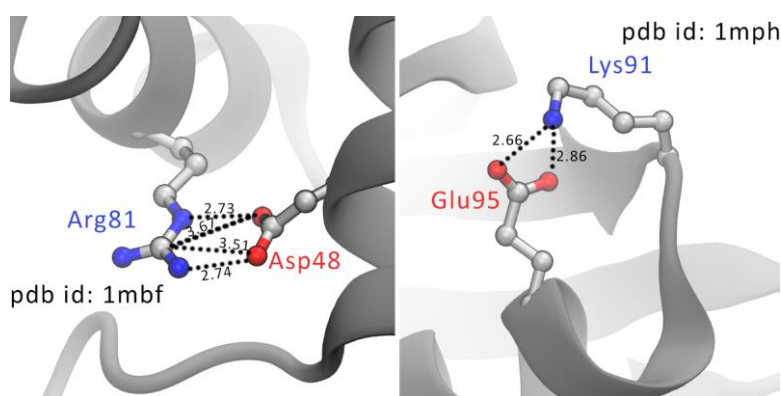


Figure S9. Examples of salt bridges involving Arg (left) and Lys(right). Key distances between the interacting residues are highlighted with dashed lines and the numerical values are given in Å. Hydrogen atoms are omitted for clarity.

Arad and co-workers^[22] reported an average N-O distance of 2.93-2.94 Å for Arg-carboxylate and 3.08-3.10 Å for Lys-carboxylate salt bridges obtained from 94 folded protein crystal structures. Donald et al.^[23] analysed 3644 X-ray structures and discovered a strong preference for Arg to interact with Asp and Glu in a bidentate fashion in a *side on* geometry (e.g. close to the sidechain at N^ε and N^{η2} as in the left panel in Fig. S9). In such salt-bridge structures, the distance between an interacting atom of a

carboxylate and the carbon atom of the guanidine moiety of Arg ($O-C^\zeta$) has a probability maximum at around 3.6-3.7 Å. Noteworthy, for interaction of Arg with a singly oxygen atom of a carboxylate the $C^\zeta-O$ distance can be as short as 3.3-3.4 Å.

Our MD simulations reveal that for the first nearest neighboring Gdm^+ with respect to the CTER that binds in a bidentate fashion (equivalent of both *side on* and *end on* motifs of Arg-carboxylate interactions) the corresponding $N^{Gdm^+}-O^{CTER}$ distance distribution peaks at ~ 2.7 Å (Fig. S10) whereas the $C^{Gdm^+}-O^{CTER}$ distance distributions have a maximum at 3.5 Å (Figure 4, top right).

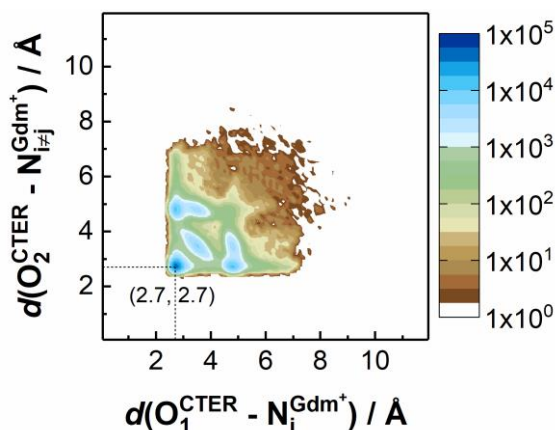


Figure S10. Combined probability distribution functions of the distances between two different oxygen atoms of CTER of GGG and two different nitrogen atoms of the 1st nearest neighboring Gdm^+ cation as obtained from MD simulations in 1 mol·L⁻¹ $GdmCl$ solutions. The position of the global probability maximum corresponding to a bidentate interaction is shown with dashed lines.

Thus, the simulated distances between the charged CTER of GGG and Gdm^+ cations are shorter than typically observed in intra-protein ionic interactions and are similar to very strongest salt bridges.^[24] Thus, assuming the (attractive and repulsive) interaction potential for Arg/Lys salt-bridges to be similar to $-COO^-Gdm^+$, the interaction energies for Gdm^+ binding to a carboxylate group is similar to that of a salt-bridge in a protein.

Polarization, charge transfer and ion-specific geometry effects on the dipole moment of GGG

To study possible polarization and charge transfer effects on the dipole moment of GGG, we have extracted representative GGG structures from our MD trajectories. For these we performed single point quantum-chemical calculations in the gas phase and in a polarizable continuum of water. The results are summarized in Table S1 and compared to values obtained from the C36m force-field. The calculations were performed using Gaussian 09 (Rev. B01)^[25] at the M05-2X/6-31+G(d,p) level of theory with ultrafine integration grid.^{[26],[27]} Atomic partial charges were estimated using Breneman's electrostatic potential fitting method CHELPG.^[28] The latter were also used to estimate the dipole moment of GGG in ion-bound structures.

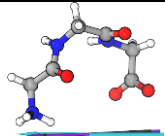
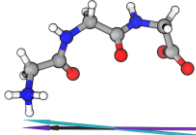
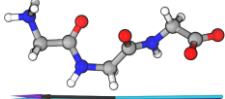
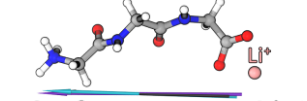
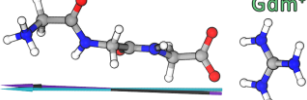
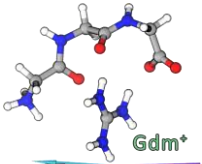
This comparison shows excellent agreement between the force-field derived dipole moment values and those calculated in a polarizable continuum (Table S1) for all the studied structures. Both are significantly larger than the corresponding gas phase values. This suggests that the C36m atomic partial charges accurately describe the polarizing effect of the medium on the solute's dipole moment.^[5,6]

Possible charge transfer effects and ion-specific geometries on the GGG dipole moment were addressed by calculating its atomic partial charges in several ion-bound configurations (three bottom rows in Table S1). Charge transfer is rather weak for the Li^+ -bound structure in the continuum solvent

and essentially vanishes for the Gdm^+ -bound structure. Moreover, the calculated dipole moment values of GGG in ion-bound configurations are very close to the values obtained for the same configurations in the absence of the cations. Thus, polarization effects due to the cation are too small to explain the observed reduction of the GGG relaxation reported in the main manuscript.

Finally, we estimate the effect of ion-specific geometries by comparing two representative Gdm^+ -bound structures: one with Gdm^+ strongly interacting with the CTER oxygen atoms and another one with Gdm^+ interacting with an oxygen atom of the CTER and the carbonyl oxygen of the central Gly-2 residue. In both cases it is apparent that the force-field derived dipole moment excellently agrees with the values calculated both with and without the bound cation within the continuum solvation model. Taken together, these results support the notion that the variation of the GGG dipole moment in aqueous salt solutions is primarily conformation-dependent.

Table S1. Comparison of the dipole moment vectors^[a], μ_{GGG} , and total charge, q_{GGG} , values of GGG calculated for selected isolated and ion-bound structures^[b,c] extracted from MD trajectories using the C36m force-field point charges and single point quantum chemical calculations at the M05-2X/6-31+G(d,p) level of theory in gas phase and in a polarizable continuum environment.

Structure	$ \mu_{\text{GGG}} , \text{D}$			q_{GGG}, e		
	C36m	M05-2X/6-31+G(d,p) ^[b]		C36m	M05-2X/6-31+G(d,p)	
		Gas	H ₂ O (SMD ^[27])		gas	H ₂ O (SMD)
	29.0	25.4	30.5	0	0	0
	40.0	34.7	40.3	0	0	0
	44.0	39.1	44.8	0	0	0
	41.6	36.2 (w/o Li ⁺ 36.4)	39.4 (w/o Li ⁺ 41.2)	0	+0.14	+0.08
	46.5	41.3 (w/o Gdm ⁺ 40.5)	46.9 (w/o Gdm ⁺ 46.1)	0	+0.07	-0.03
	36.7	30.8 (w/o Gdm ⁺ 31.9)	36.5 (w/o Gdm ⁺ 37.0)	0	+0.07	+0.01

^[a]The direction of the μ_{GGG} vector is shown with arrows next to each structure. The dipole moment vectors obtained from C36m, M05-2X/6-31+G(d,p) gas and solvated calculations are shown in violet, black and cyan, respectively.

^[b]For the ion-bound structures calculated at the M05-2X/6-31+G(d,p) level of theory, the total charge of GGG was calculated by summing up the atomic partial charges obtained by the electrostatic potential fitting method CHELPG.^[28] The same charges were used to calculate the dipole moment vectors μ_{GGG} with respect to the GGG center of mass.

^[c]The same ion-bound structures were also calculated without the cation and the corresponding dipole moment values are also shown.

Supporting References

- [1] W. Ensing, J. Hunger, N. Ottosson, H. J. Bakker, *J. Phys. Chem. C* **2013**, *117*, 12930–12935.
- [2] V. Balos, M. Bonn, J. Hunger, *Phys. Chem. Chem. Phys.* **2015**, *17*, 28539–28543.
- [3] E. A. S. Cavell, P. C. Knight, S. M. A., *Trans. Faraday. Soc* **1971**, *67*, 2225.
- [4] J. C. Phillips, R. Braun, W. Wang, J. Gumbart, E. Tajkhorshid, E. Villa, C. Chipot, R. D. Skeel, L. Kalé, K. Schulten, *J. Comput. Chem.* **2005**, *26*, 1781–1802.
- [5] J. Huang, S. Rauscher, G. Nawrocki, T. Ran, M. Feig, B. L. De Groot, H. Grubmüller, A. D. MacKerell, *Nat. Methods* **2016**, *14*, 71–73.
- [6] R. B. Best, X. Zhu, J. Shim, P. E. M. Lopes, J. Mittal, M. Feig, A. D. MacKerell, *J. Chem. Theory Comput.* **2012**, *8*, 3257–3273.
- [7] W. Humphrey, A. Dalke, K. Schulten, *J. Mol. Graph.* **1996**, *14*, 33–38.
- [8] S. Bykov, S. Asher, *J. Phys. Chem. B* **2010**, *114*, 6636–6641.
- [9] M. R. Shirts, D. L. Mobley, J. D. Chodera, V. S. Pande, *J. Phys. Chem. B* **2007**, *111*, 13052–13063.
- [10] T. Darden, D. York, L. Pedersen, *J. Chem. Phys.* **1993**, *98*, 10089–10092.
- [11] J. P. Ryckaert, G. Ciccotti, H. J. C. Berendsen, *J. Comput. Phys.* **1977**, *23*, 327–341.
- [12] S. Miyamoto, P. A. Kollman, *J. Comput. Chem.* **1992**, *13*, 952–962.
- [13] M. P. Allen, D. J. Tildesley, *Computer Simulation of Liquids*, Clarendon Press, **1989**.
- [14] G. J. Martyna, D. J. Tobias, M. L. Klein, *J. Chem. Phys.* **1994**, *101*, 4177–4189.
- [15] S. E. Feller, Y. Zhang, R. W. Pastor, B. R. Brooks, *J. Chem. Phys.* **1995**, *103*, 4613–4621.
- [16] J. A. Drake, B. M. Pettitt, *J. Comput. Chem.* **2015**, *36*, 1275–1285.
- [17] R. Schweitzer-Stenner, F. Eker, Q. Huang, K. Griebenow, *J. Am. Chem. Soc.* **2001**, *123*, 9628–9633.
- [18] W. Wachter, Š. Fernandez, R. Buchner, G. Hefter, *J. Phys. Chem. B* **2007**, *111*, 9010–9017.
- [19] V. Balos, H. Kim, M. Bonn, J. Hunger, *Angew. Chemie Int. Ed.* **2016**, *55*, 8125–8128.
- [20] J. Paterová, K. B. Rembert, J. Heyda, Y. Kurra, H. I. Okur, W. R. Liu, C. Hilty, P. S. Cremer, P. Jungwirth, *J. Phys. Chem. B* **2013**, *117*, 8150–8158.
- [21] L. Fielding, *Prog. Nucl. Magn. Reson. Spectrosc.* **2007**, *51*, 219–242.
- [22] B. Musafia, V. Buchner, D. Arad, *J. Mol. Biol.* **1995**, *254*, 761–770.
- [23] J. E. Donald, D. W. Kulp, W. F. DeGrado, *Proteins Struct. Funct. Bioinforma.* **2010**, *79*, 898–915.
- [24] S. Kumar, R. Nussinov, *Biophys. J.* **2002**, *83*, 1595–1612.
- [25] M. J. Frisch, G. W. Trucks, H. B. Schlegel, G. E. Scuseria, M. A. Robb, J. R. Cheeseman, G. Scalmani, V. Barone, B. Mennucci, G. A. Petersson, et al., *Gaussian 09, Revis. B.01, Gaussian, Inc., Wallingford CT* **2009**.
- [26] Y. Zhao, D. G. Truhlar, *Acc. Chem. Res.* **2008**, *41*, 157–67.
- [27] A. V Marenich, C. J. Cramer, D. G. Truhlar, *J. Phys. Chem. B* **2009**, *113*, 6378–6396.
- [28] C. M. Breneman, K. B. Wiberg, *J. Comput. Chem.* **2018**, *11*, 361–373.